

Joint Impacts of Acidity and Viscosity on the Formation of Secondary Organic Aerosol from Isoprene Epoxydiols (IEPOX) in Phase Separated Particles

Yue Zhang*,†,‡ Yuzhi Chen,† Ziying Lei,§ Nicole E. Olson,|| Matthieu Riva,⊥ Abigail R. Koss,‡ Zhenfa Zhang,† Avram Gold,† John T. Jayne,‡ Douglas R. Worsnop,‡ Timothy B. Onasch,‡ Jesse H. Kroll,‡,§,¶ Barbara J. Turpin,† Andrew P. Ault,*,§,|| and Jason D. Surratt*,†

†Department of Environmental Sciences and Engineering, Gillings School of Global Public Health, University of North Carolina at Chapel Hill, Chapel Hill, North Carolina 27599, United States

‡Aerodyne Research Inc., Billerica, Massachusetts 01821, United States

§Department of Environmental Health Sciences, School of Public Health, University of Michigan, Ann Arbor, Michigan 48109, United States

||Department of Chemistry, College of Literature Sciences and the Arts, University of Michigan, Ann Arbor, Michigan 48109, United States

⊥Univ Lyon, Université Claude Bernard Lyon 1, CNRS, IRCELYON, F-69626 Villeurbanne, France

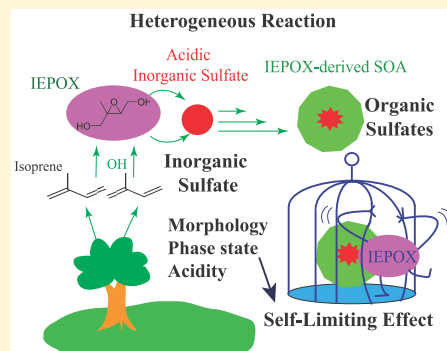
¶Department of Civil and Environmental Engineering, Massachusetts Institute of Technology, Cambridge, Massachusetts 02139, United States

§,¶Department of Chemical Engineering, Massachusetts Institute of Technology, Cambridge, Massachusetts 02139, United States

Supporting Information

ABSTRACT: Isoprene-derived secondary organic aerosol (SOA) is mainly formed through acid-catalyzed reactive uptake of isoprene-derived epoxydiols (IEPOX) onto sulfate aerosol particles. The effect of IEPOX-derived SOA on the physicochemical properties of existing aerosols and resulting capacity for further SOA formation remains unclear. This study systematically examined the influences of IEPOX-derived SOA on the phase state, morphology, and acidity of pre-existing sulfate aerosol particles, as well as their implications on the reactivity and evolution of these particles. By combining aerosol thermodynamic and viscosity modeling, our predictions show that aerosol viscosity and acidity change drastically after IEPOX reactive uptake, with the aerosol becoming less acidic (increasing by up to 1.5 pH units) and more viscous by 7 orders of magnitude, thereby significantly reducing the diffusion time scale of the molecules inside the particles. Decreased aerosol acidity and increased viscosity co-contribute to a self-limiting effect where newly formed IEPOX-derived SOA inhibits additional multiphase chemical reactions of IEPOX. The relative contribution to the inhibitory effect of pH versus viscosity depends on the initial ratio of the IEPOX-to-inorganic sulfate aerosol, which differs between geographic regions. Moreover, reduced aerosol acidity and increased kinetic limitation to diffusion leading to lower hydronium ions and slower mixing times may impede other multiphase chemical processes after the formation of IEPOX-derived SOA. This study highlights important interconnections between physical and chemical properties of aerosol particles that come from interactions of inorganic and organic components, which jointly influence the evolution of atmospheric aerosols.

KEYWORDS: Secondary Organic Aerosol, Isoprene, IEPOX, Phase Separation, Viscosity, Acidity



1. INTRODUCTION

Fine particulate matter (PM_{2.5}) is known to have significant effects on air quality, climate, and human health.¹ Secondary organic aerosol (SOA) formed through the oxidation of volatile organic compounds (VOCs) comprises a large percentage of PM_{2.5} mass in both field measurements and laboratory experiments.^{2–5} As the non-methane VOC with the highest global emission rate, isoprene is also oxidized in the

atmosphere to form significant amounts of SOA,^{6,7} including through acid-catalyzed reactive uptake (or multiphase

Special Issue: New Advances in Organic Aerosol Chemistry

Received: July 26, 2019

Revised: October 31, 2019

Accepted: October 31, 2019

Published: October 31, 2019

chemistry) of isoprene epoxydiols (IEPOX) onto sulfate aerosol particles.^{8,9} The uptake coefficient of this reaction can be calculated by dividing the number of molecules lost to the surface with the total number of molecules striking the surface. Due to the relatively high reactive uptake coefficient of IEPOX onto existing sulfate particles, this process has been found to lead to substantial amounts of PM_{2.5}, especially in forested areas with broadleaf trees such as the Southeastern United States and the Amazon rainforest.^{10–12} Due to relatively large mass loadings of IEPOX-derived SOA in these areas, the physicochemical properties of IEPOX-derived SOA particles may have a significant influence on the subsequent formation and evolution of organic PM_{2.5}.^{13,14} Despite recent studies revealing the detailed reaction mechanisms of these multiphase chemical processes, few have explored whether IEPOX-derived SOA will alter the physicochemical properties of PM_{2.5}.^{15,16}

As one of the important physicochemical properties, the phase state of aerosol particles can change from liquid to semisolid and even solid states, which can be quantified by the viscosity.^{17,18} Depending on the environment that the aerosol particles are in, the viscosity of the PM_{2.5} can change over 12 orders of magnitude, from aqueous to glassy-like.^{19,20} Changes in viscosity can increase the diffusion time scales of molecules within the particles from microseconds to days or even weeks, with the implications of slowing down acid-catalyzed heterogeneous reactions,^{14,15} particle growth,²¹ and particle aging processes.^{22–24} Sometimes the viscous organic components of an aerosol may undergo phase separation from inorganic species, forming a layer (i.e., shell) at the edge of the inorganic components, referred to as core–shell morphology.^{25–28} This shell can reduce the reactive uptake of molecules into the aqueous inorganic core,^{14,29,30} and even creating a potential self-limiting effect during the reactive uptake process.^{15,28,31} The viscosity of the core can also increase after multiphase or particle phase reactions, further limiting multiphase chemistry.¹⁶ The combination of aerosol phase state, morphology, and interactions between organic and inorganic phases influences the lifecycle of the aerosols,³² including the heterogeneous uptake of IEPOX,^{14,15,33} HO₂,³⁴ OH,³⁵ and N₂O₅^{29,36,37} and thus needs to be carefully investigated.

Aerosol pH also governs the partitioning and reactions of semivolatile species between the gas and particle phases, as well as within the particle phase. Many atmospheric processes, including the gas–particle equilibrium of NH₃ and HONO,^{38,39} the hydrolysis of organic nitrates,⁴⁰ and the reactive uptake of IEPOX to form SOA, such as the formation of organosulfates (OSs), all depend on aerosol pH values.^{41,42} However, direct measurement of aerosol pH in the particle phase is challenging and thus rare. At present, such measurement can only be obtained for simple supermicrometer or submicrometer particles exposed to high relative humidity rather than complex submicrometer SOA particles.^{43–45} Highly parametrized thermodynamic and phase-partitioning models for estimating the pH of submicrometer particles are useful, but limited by the species contained (e.g., limited organic species) and reliance on the gas-particle system being at thermodynamic equilibrium without considering the kinetic limitations such as coating effects.^{46,47} It has been shown that pH changes can drive phase separation and the pH values between the two phases at equilibrium are less than one-unit difference when there is liquid–liquid phase separa-

tion.^{48,49} However, few studies have provided a method for estimating the particle pH when organic–inorganic interactions happened during the course of reactions, especially when the organic phase is viscous.⁵⁰ Thus, measurements are needed for the evolution of such interactions within particles to determine effects on physicochemical properties and chemical reactivities.

To provide detailed insights into the implications of aerosol phase state and pH during the multiphase formation of isoprene-derived SOA, experimental data combined with in-house models that consider the interactions between the organic and inorganic components, as well as the implications of such interactions on the aerosol phase, pH, and reactivity, are presented. These customized models used data from a series of laboratory experiments with IEPOX-to-inorganic sulfate ratios that mimic conditions in the Southeastern United States and Amazon rainforest regions, which characterize the self-limiting effects during IEPOX-derived SOA formation. Our model results demonstrate that the multiphase reactions between gas–particle and subsequent interactions between the organic and inorganic phases have significant impacts on the predicted aerosol viscosity and pH, leading to suppressions of further acid-catalyzed multiphase chemical reactions with IEPOX and likely explaining the experimentally observed self-limiting effect of IEPOX on SOA formation.

2. METHODS

2.1. Chamber Experiments. Experiments were performed in the indoor environmental chambers at the University of North Carolina at Chapel Hill (UNC) and Massachusetts Institute of Technology (MIT). The experimental setup and analytical techniques used in this work have been described in detail previously^{13,51–53} as well as in the *Supporting Information (SI)* and *Figure S1*. The operating conditions for the UNC and MIT chambers were identical except that the UNC chamber was operated at 50% RH whereas the MIT chamber was operated at <5% RH. Briefly, acidic sulfate particles were atomized into the chamber using mixed aqueous solutions of 0.06 mol L^{−1} of ammonium sulfate and 0.06 mol L^{−1} sulfuric acid. Gas phase IEPOX was injected in through a heated manifold after the seed particle concentrations were stabilized and the chamber was dark with no strong oxidants. The *trans*-β-IEPOX was synthesized in house with detailed procedures described elsewhere.⁵⁴ Experimental conditions that simulate the ratio of gas phase IEPOX (μg m^{−3}) to inorganic sulfate aerosol (μg m^{−3}) (or IEPOX:SO₄^{2−} ratio) in the Southeastern United States and the Amazon rainforest were employed, noted as the ratios representing the Southeastern United States and Amazon regions, respectively, with detailed experimental procedures described by Riva et al.¹⁵ The Southeastern United States experiment has a lower IEPOX:SO₄^{2−} ratio of 1.5 while the Amazon experiment has a higher IEPOX:SO₄^{2−} ratio of 10.5. These ratios were achieved by adjusting both the mass concentrations of inorganic sulfate seed particles and gas-phase IEPOX.¹⁵

During the course of the experiments, IEPOX-derived SOA was collected using a Particle into Liquid Sampler system (PILS; BMI model 4001). The inorganic sulfate from the PILS vials were analyzed by ion chromatography (IC). The organic components of IEPOX-derived SOA, such as the 2-methyltetros (2-MTs), 2-methyltetrol sulfates (or 2-methyltetrol organosulfates, 2-MT-OS), and 2-methyltetrol sulfate dimers (2-MT-OS dimer),^{9,55,56} in each PILS vial were also

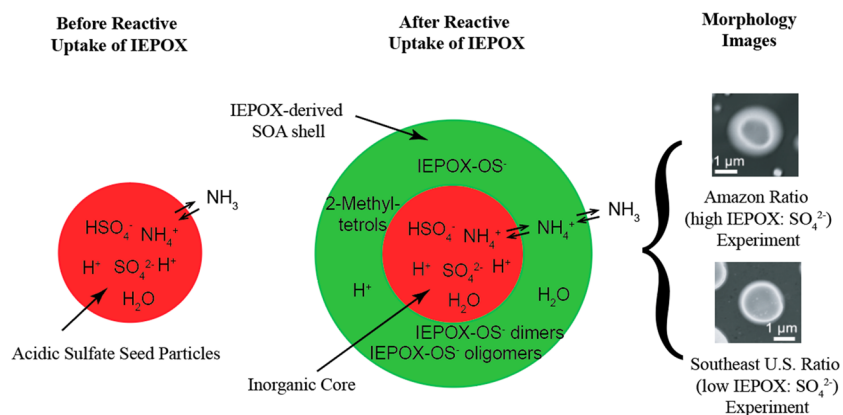


Figure 1. Schematic of the model framework for pH and viscosity estimation. The left panel shows that the acidified ammonium sulfate particles before IEPOX injection are homogeneously mixed. The middle panel shows that the model assumes organic–inorganic phase separation, with inorganic species in the core and organic species in the shell. The right panel shows the actual microscopic images of the aerosol particles collected during the experiments, confirming that these particles were indeed phase separated as indicated in the middle panel of the figure. All simulations were run at a 50% RH condition where the particles contain a certain amount of water (especially the aqueous core) based on the hygroscopicity of each phase.

analyzed by ultraperformance liquid chromatography interfaced to electrospray ionization high-resolution quadrupole time-of-flight mass spectrometry (UPLC/ESI-HR-QTOFMS) to obtain the concentration of each compound in the particle phase. Herein, IEPOX-OS is used as an abbreviation to represent the 2-methyltetrols as well as the 2-methyltetrols dimers, trimers, and oligomers thereof. The time series values of the particle constituents at the above two conditions were reported by Riva et al. and were used as constraints for the modeling section of this research article.¹⁵

2.2. Microscopy Imaging. Aerosol particle samples were collected before, during, and after IEPOX reactive uptake to confirm the mixing states and phase states (i.e., homogeneous or core–shell structure morphologies) using a three-stage microanalysis particle sampler (MPS-3, California Measurements, Inc.) with d_{50} size cuts of 5.0, 2.8, and 0.4 μm that was operated at 2.1 LPM. Particles were impacted onto silicon wafer substrates (Ted Pella, Inc.) and carbon-type-b Formvar-coated copper transmission electron microscopy (TEM) grids. Only samples from the third stage ($<0.40\ \mu\text{m}$) of the impactor were analyzed because the size range of this stage included the sizes of the aerosol particles generated in the chamber. Samples were stored in the dark in sealed plastic vials at room temperature prior to analysis.⁵⁷ Particles on silicon substrates were imaged in $5 \times 5\ \mu\text{m}^2$ regions by atomic force microscopy (AFM; PicoPlus 5500 atomic force microscope; Agilent, Santa Clara, CA) that operated at a 40 N/m spring constant and 300 kHz resonant frequency. The height images were obtained by performing tapping mode utilizing Aspire CT300R probes (NanoScience, AZ). The original images collected were at 512 pixels per line and acquired as $5 \times 5\ \mu\text{m}^2$ or $10 \times 10\ \mu\text{m}^2$ areas with line scans of 0.75 Hz and then cropped. Raw data was processed using SPIP 6.2.6 software (Image Metrology, Hørsholm, Denmark) to measure particle height and radius. Scanning electron microscopy (SEM) images were also obtained by examining particles using a FEI Helios 650 Nanolab-Dualbeam electron microscope equipped with a high angle annular dark field (HAADF) detector operated at an accelerating voltage of 10.0 kV, a current of 0.80 nA, and pressures ranging from 10^{-3} to 10^{-5} Pa.

2.3. Modeling Viscosities of IEPOX-Derived SOA Mixed with Inorganic Aerosol Constituents.

The

viscosities of the SOA mixture with inorganic aerosol constituents were first calculated by obtaining the glass transition temperatures of individual organic and inorganic species based on the molecular composition method of DeRieux et al.,⁵⁹ which is described in the [SI](#) and [Table S3](#). The glass transition temperatures of the inorganic core and organic shell were calculated separately, based on AFM and SEM images shown in [Figure 1](#). The average glass transition temperatures were calculated by adding the components together based on the core–shell morphology and mass fractions of each component.^{60,61} By assuming that water transported freely between the organic shell and the inorganic core, the model then calculated the glass transition temperatures of the organic shell and the inorganic core mixed with water individually by considering the hygroscopicity (κ) of the two phases. The water-included glass transition temperatures were then converted to viscosities of organic and inorganic phases based on the Vogel–Tammann–Fulcher (VTF) equation, the fragilities of the organic compound, and the ambient temperature, as shown in the [SI](#). The above procedure was applied to the laboratory data to calculate the time-series viscosities of the inorganic and organic layers that consisted of sulfates and the IEPOX-derived SOA generated at the two different IEPOX:SO₄²⁻ ratios, as shown in Riva et al.¹⁵ The glass transition temperature calculation results of each IEPOX-derived SOA constituent, including 2-MTs, 2-MT-OS, and 2-MT-OS dimers, are shown in [Table S1](#). The viscosity estimation of the aerosols was based on all the above species combined. The mass percentages of 2-MT and 2-MT-OS (including oligomers) in the IEPOX-derived SOA were assumed to be 33.4% and 66.6%, respectively, based on a previous study.⁵⁶ A sensitivity study of various modeling scenarios, including the homogeneous mixture of the inorganic and organic components, were summarized in [Table S2](#). Gordon–Taylor parameters between all IEPOX-derived SOA and water, IEPOX-derived SOA constituents, and IEPOX-derived SOA with inorganic sulfate were assumed to be 2.5, 1, and 1.4, respectively, based on previous studies.^{59,62–64} The viscosity values calculated were based on the 50% RH experiment performed at the UNC chamber, with an uncertainty range up to 1.5–2 orders of magnitude.¹⁵

2.4. Modeling of the pH of IEPOX-Derived SOA (Thermodynamic Model Considering Organosulfates)

The pH of aerosol particles during the reaction processes was calculated using an in-house thermodynamic model with four modeling scenarios (I–IV), with details described in Figures 1 and S2, and Table S3. Each model scenario used measured time-series inorganic sulfate concentrations from the PILS-IC, total sulfate concentrations and the NH_4^+ concentrations from the Aerosol Chemical Speciation Monitor (ACSM, Aerodyne Research Inc.) as well as the size of the particles from Scanning Electrical Mobility Spectrometer (SEMS, Brechtel Inc.) as input values, as shown in Figure S1.⁶⁵ The proton balance equation together with the mass balance equations for H^+ , NH_4^+ , SO_4^{2-} , and HSO_4^- as well as the IEPOX-OS (including 2-MT-OSs, 2-MT-OS dimers, and 2-MT-OS oligomers) were built into this model as multivariable equations to solve the H^+ ion activity, as shown in eq S1–S7. The activity coefficients of the inorganic and the organic phases used in the model were derived from ammonium bisulfate and organic mixtures measured from the midpoint of experiments, respectively. We found the activity coefficients mostly changed within 1 order of magnitude when considering the variations of the inorganic and organic species during the course of the experiments, resulting in the pH values changing within 1 unit. Therefore, we used constant activity coefficients to calculate the pH values with the associated uncertainty range less than 1 unit. The output of the model was the activity of each ion, where pH was calculated as the negative logarithm of the hydrogen ion activity (a_{H^+}). Scenario I was used as the main framework of this model, which assumed IEPOX-derived SOA particles underwent phase separation, as shown by the microscopic images in the Results and Discussion, with the inorganic sulfate in the core and the organic compounds (including organic sulfates) in the shell. Due to the energy barrier, differences in mass concentrations, and possible nonequilibrium state between the aqueous inorganic core and the semisolid organic shell as IEPOX continued to react with the inorganic sulfate, the activities of NH_4^+ and H^+ in the core and in the shell were likely to have gradients.⁴⁹ Thus, a gradient Q between the activities of NH_4^+ and H^+ in the core and in the shell was defined, with details and calculated Q values at different stages of the experiment shown in eq S8 and Table S4. Scenarios II and III were used as typical scenarios for models that assumed that the inorganic and organic aerosol components were homogeneously mixed, with Scenario II considering the first-order proton dissociation of all IEPOX-OS and Scenario III not considering any IEPOX-OSs. The difference between Scenarios II and III was that Scenario III only considered inorganic species when calculating the pH values and did not take the disassociation of IEPOX-OS into account. Scenario IV assumed that the particles only consisted of either the organic compounds or the inorganic compounds, which served as a reference point for the acidity and viscosity calculations. A schematic diagram and detailed assumptions of each model scenario are listed in Figure S2, and Tables S2 and S3, respectively. The gas-particle balance of NH_3 and NH_4^+ was calculated using a Henry's law constant of 0.0161 atm M^{-1} .⁶⁶ Growth factors of 1.2 and 1.02 at 50% RH were used to calculate the liquid water content of the inorganic and organic aerosol components, respectively.^{67,68} The assumed growth factors matched the experimental SEMS data. The mean activity coefficients for the ammonium bisulfate inorganic core and 2-methyltetrol (representing the organic shell) were

calculated based on Aerosol Inorganic–Organic Mixtures Functional groups Activity Coefficient (AIOMFAC, version 2.31, <https://aiomfac.lab.mcgill.ca/index.html>) and Extended-Aerosol Inorganics Model (E-AIM, June 2017 version, <http://www.aim.env.uea.ac.uk/aim/model2/model2a.php>),^{69–72} in agreement with the activity coefficients of ammonium bisulfate and organic components reported in previous studies.^{70,73} It is worth noting that, due to limited knowledge on the activity coefficients of organosulfate species, 2-methyltetrol was used as a surrogate to estimate the activity coefficients of IEPOX-OS (2-methyltetrol sulfates as well as their dimers and trimers). The uncertainties associated with the activity coefficients of IEPOX-OS may change the calculated pH values of the aerosols by 1–2 units due to the constant activity coefficients used in the model and the unavailability of the interactions between the organosulfates and the inorganic salts. Therefore, future studies incorporating real-time activity coefficients based on the composition at each time step of the experiment is needed; however, it will likely not change the general trend of the pH during the course of the reaction nor the conclusions of this research.

3. RESULTS AND DISCUSSION

3.1. Self-Limiting Effects of IEPOX-Derived SOA Formation.

As shown in Figure 2, an initial experiment of gaseous IEPOX reacting with ammonium bisulfate (ABS) aerosols simulating the ratio of IEPOX: SO_4^{2-} in the

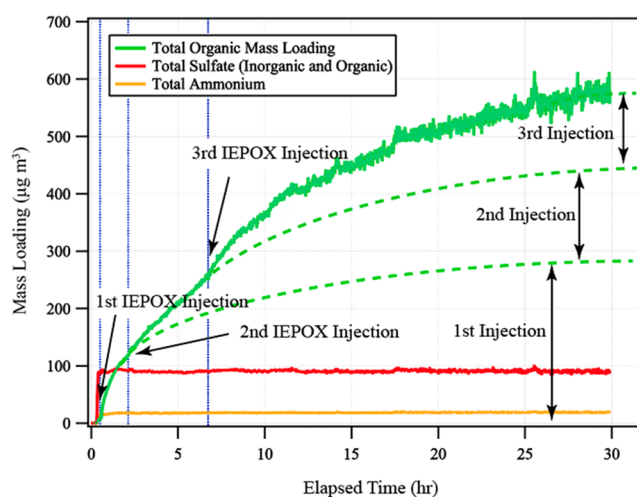


Figure 2. Laboratory data generated at the MIT environmental chamber shows the self-limiting effect of IEPOX to form SOA under an IEPOX: SO_4^{2-} ratio mimicking the conditions of the Amazon. The mass concentrations of each group of species were measured by using the aerosol mass spectrometer (AMS, Aerodyne Research Inc.). The times of each IEPOX aliquot injected into the chamber to react with acidic sulfate aerosol particles are indicated in the plot by a single-headed arrow, with the first injection at $t = 0.5$ h. The dashed vertical lines indicate when the injections of the IEPOX started. The approximate equilibration mass concentration of IEPOX-derived SOA formed from each injection of IEPOX is also indicated in the plot with green dashed lines and double-headed arrows, assuming the reaction was pseudo-first order. The IEPOX-derived SOA formed from the second and third injections are significantly lower than the first injection, indicating a self-limiting effect of IEPOX-derived SOA on additional multiphase chemical processing of gaseous IEPOX. The mass concentrations reported above have been corrected with wall loss and dilution.

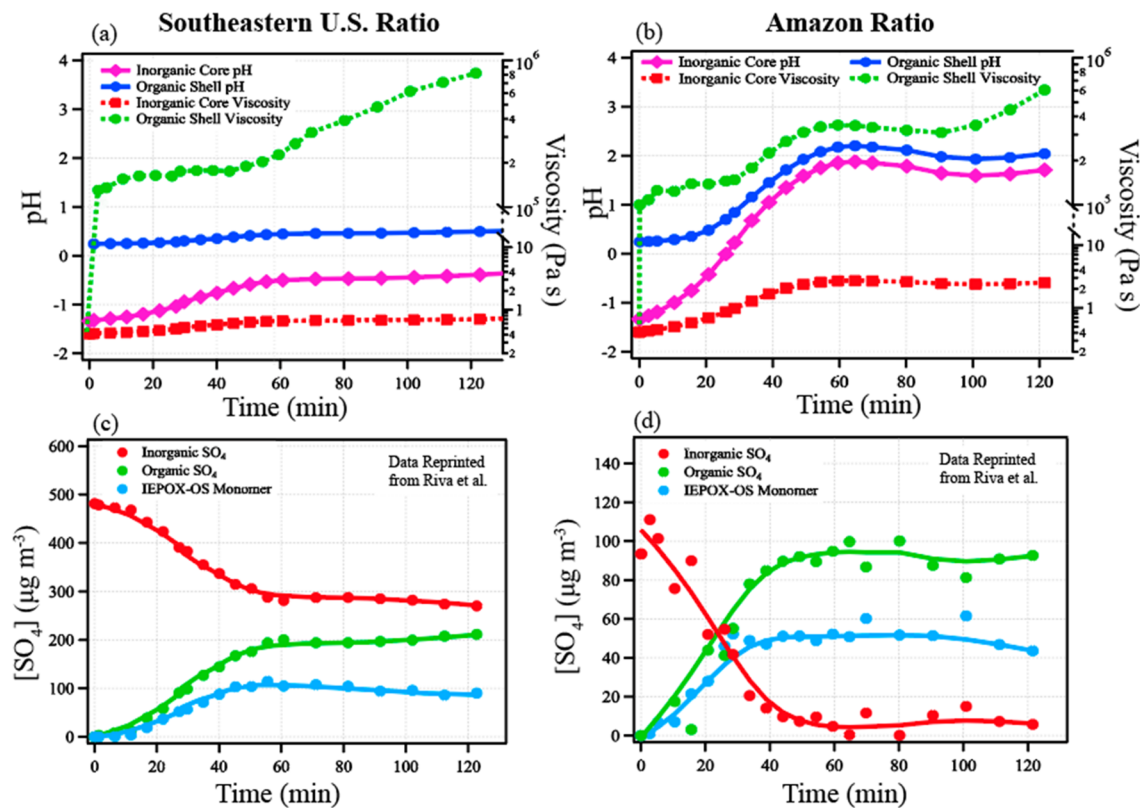


Figure 3. Time-series plot of the aerosol pH values modeled by the thermodynamic model Scenario I (assuming phase separation) during the course of (a) a low IEPOX:SO₄²⁻ ratio experiment that mimics conditions in the Southeastern United States and (b) a high IEPOX:SO₄²⁻ ratio experiment that mimics conditions in the Amazon that were performed in the UNC environmental chamber. The acidity and viscosity were modeled based on an environmental temperature of 298 K. Pink diamonds and blue dots represent the estimated pH of the inorganic core and the IEPOX-derived SOA shell, respectively. Orange squares and green dots represent the estimated viscosity of the inorganic core and the IEPOX-derived SOA shell, respectively. The pH and the viscosity values at $t = 0$ were only calculated for the pure ammonium bisulfate seed particles, as the IEPOX-SOA only formed starting from the second data point. The trend lines (both solid and dashed) are also shown in the plot. Panels (c) and (d) are the aerosol composition data to illustrate the composition-induced pH and viscosity changes. Red, green, and cyan dots represent inorganic sulfate, total OSs, and 2-MT-OSs (or IEPOX-OS monomer), respectively. Panels (c) and (d) were reproduced with permission from ref 15. Copyright 2019 American Chemical Society.

Amazonian rainforest was performed in the MIT environmental chamber at <5% RH under dark conditions. After injecting $\sim 90 \mu\text{g m}^{-3}$ ABS into the chamber and waiting for the concentration of ABS to stabilize, 2 mg of IEPOX (equivalent to 55 ppb of IEPOX) was injected into the chamber to react with the ABS particles. At 1.75 and 5.75 h after the initial injection, an additional two aliquots (each is ~ 2 mg) of IEPOX were injected into the environmental chamber to study the effects of pre-existing IEPOX-SOA on the reactive uptake of additional IEPOX. As reported previously,⁵⁵ IEPOX reacts with acidic sulfate particles through acid-catalyzed multiphase reactions to form SOA and the consecutive IEPOX-derived SOA. However, as shown in Figure 2, the amount of additional IEPOX-derived SOA formed from the subsequent injections of IEPOX decreased drastically after the initial injection, suggesting a self-limiting effect of IEPOX-derived SOA on additional multiphase chemistry. Morphology, viscosity, and the pH of aerosol particles are three factors thought to influence the acid-catalyzed multiphase chemical process leading to IEPOX-derived SOA and thus manifest as a self-limiting effect. Similar experiments were also conducted in the UNC chamber with two IEPOX:ABS ratios (1.5 for Southeastern United States and 17.1 for Amazon) at 50% RH. The experimental data obtained from the UNC Chamber were

then used as constraints in the models to examine the self-limiting effect of IEPOX in forming SOA.

3.2. Morphology of SOA-Coated Acidic Sulfate Particles. SEM and AFM images demonstrate core–shell particle morphology after acidic sulfate particles were exposed to IEPOX at 50% RH. Figures 1 and S3 show SEM and AFM images, respectively, of acidic sulfate particles after exposure to gaseous IEPOX. Particles with volume equivalent diameters of ~ 75 – 300 nm (based on projected area diameters of 300–1000 nm and typical spreading ratios)^{74,75} exhibit phase separation after exposure to IEPOX for all samples analyzed. The morphological information obtained by SEM confirms that the uptake of IEPOX onto the acidic sulfate particles leads predominantly to core–shell morphology. In addition, height traces and amplitude AFM images of particles with core–shell morphologies are included in Figure S3. Particles generated from higher IEPOX:SO₄²⁻ ratios (i.e., mimicking the Amazonian conditions) lead to thicker organic coatings compared with low IEPOX:SO₄²⁻ ratios (i.e., mimicking Southeastern United States conditions). Because the particles were collected following the same impaction procedures, the particle heights analyzed by the AFM also indicate the average aerosol viscosity: a taller height profile is likely associated with a more viscous particle while a shorter height profile is likely associated with a less viscous particle, agreeing with those

findings in Riva et al.¹⁵ Figure S3 shows that the AFM particle heights formed from the Amazonian ratio experiments were more than 50% taller than those produced in the Southeastern United States ratio experiments, likely due to a more rapid conversion of aqueous inorganic sulfate to organic components. The results above demonstrate that the aerosols generated under both the Amazon and Southeastern United States ratios have core–shell morphology, suggesting that Scenario I can be used to model the pH values of these phase separated aerosol particles.

3.3. Effects of Aerosol Composition and Mixing State on Aerosol Phase State and pH. Based on the core–shell morphologies determined by microscopy and the molecular composition of IEPOX-derived SOA obtained by chemical characterization, a core–shell viscosity and thermodynamic model were constructed to estimate the values and trends of viscosity and pH as IEPOX heterogeneously reacted with ABS particles throughout the course of each experiment. The atmospheric implications of such transitions were analyzed by a kinetic model that was used in previous research.¹⁴

3.3.1. Effects of Aerosol Composition on Model Predictions of Aerosol pH. By converting inorganic sulfate to organosulfur forms (OS), acid-catalyzed multiphase chemistry of IEPOX also alters the chemical composition of inorganic and organic species in the aerosols. This conversion potentially alters the acidity of the aerosol particles. IEPOX-derived OSs have been characterized recently by hydrophilic interaction liquid chromatography interfaced to ESI-HR-MS (HILIC/ESI-HR-MS) methods^{56,76} and were demonstrated to be the dominant mass fraction of IEPOX SOA during laboratory and field studies.^{56,77} Commonly utilized aerosol thermodynamic models assume sulfate only as inorganic sulfur;^{65,78} hence, exclusion of particulate OSs from thermodynamic predictions may lead to issues with pH estimations. When calculating the pH derived from data obtained from field or laboratory studies, such models may incorrectly reduce the H^+ concentration by only considering the charge balance and acid dissociation constants (pK_a) of inorganic species, especially when substantial amounts of OSs are mischaracterized as inorganic sulfate. Hence, the response of condensed-phase acidity to the reactive uptake of IEPOX was investigated by applying the aerosol composition time series data from the UNC chamber experiments described above to the model framework of Scenario I, which takes OSs into consideration.

Figure 3a and b shows pH and viscosity changes of the particle core and shell under the Southeastern United States and Amazon conditions when considering the effects of phase separation between the organic sulfate and inorganic sulfate phase under Scenario I, respectively. Figure 3c and d shows the reprinted chemical composition trend of each species reported by Riva et al. under the Southeastern United States ratio and the Amazon ratio, respectively.¹⁵ The model reveals that the initial pH value of the inorganic core is ~2 pH units lower than that of the organic shell, as a consequence of the core consisting of more acidic bisulfate ions as well as the core and shell possibly not reaching equilibrium yet because IEPOX-SOA is still forming rapidly during the first 30 min of the experiments. The estimated pH of the ammonium bisulfate particles at the beginning of the experiment from this thermodynamic model agrees well with the result obtained from either the AIOMFAC and E-AIM models,^{69,70} suggesting the validity of the in-house model. The inorganic sulfate

aerosols were also collected onto pH paper based on the method by Craig et al.,⁴³ and the measured pH agrees with the thermodynamic model results as well. As the reactive uptake of the IEPOX to the acidic sulfate particles continues, pH values of the inorganic core and organic shell both increase but with different magnitudes. In addition, pH values of aerosols generated using IEPOX: SO_4^{2-} ratios mimicking Amazon conditions change much more dramatically than those mimicking the Southeastern United States conditions. This difference between these two sets of pH values is caused by a higher conversion rate of inorganic sulfate to organic sulfate under Amazonian conditions. As a reference, the results of Scenarios II and III modeling homogeneously mixed aerosols, which are similar to traditional models, are also shown in Figure S4. The modeling results demonstrate that the pH values of the phase-separated particle scenario have higher core acidities and lower shell acidities when compared with the homogeneously mixed particle scenario. It is worth noting that there is likely some exchange of the inorganic and organic species between the core and the shell, so the actual pH of the aerosols may lie between Scenarios I and II, but lean more toward Scenario I as the phase separation was still observed. The comparison between Scenarios II and III also demonstrates that large and likely unrealistic increases of aerosol pH occur when OS disassociation reactions are not taken into account in the model, especially under conditions that mimic the Amazon where inorganic sulfate was largely converted to OS species. Finally, a sensitivity analysis on the acidity estimation was conducted by varying the pK_a values of the IEPOX-derived OSs, and this is shown in Figure S5. The results show that the core acidity remains stable for the Southeastern U.S. condition while the shell acidity changes by 2–4 pH units, suggesting the importance of further research on the role of these IEPOX-derived SOA components in governing aerosol shell acidity, and thus, reactivity on the aerosol surface.

3.3.2. Effect of Aerosol Composition on Its Phase State. The modeling procedure was applied to the laboratory data to calculate the time-series viscosity of the organic layer that consisted of the IEPOX-derived SOA generated at the two different IEPOX: SO_4^{2-} ratios, as shown in Riva et al.¹⁵ and illustrated in Figure 3.

Figure 3a and b shows viscosity changes of the particle core and shell under the Southeastern United States and Amazon conditions, respectively. As the acid-catalyzed multiphase chemistry of IEPOX continues, the organic layer appears and its viscosity increases from 10^5 Pa s to nearly 10^6 Pa s, suggesting more viscous species forming by the end of each experiment. Such increases in viscosity are driven by the formation of highly viscous species, especially the large mass fractions of IEPOX-derived OSs and oligomers produced in these aerosols. As previously reported, IEPOX-derived SOA can be treated as effectively nonvolatile under most relevant atmospheric conditions.^{79,80} A recent study by Zhang et al. shows that the uptake of IEPOX by acidic sulfate cores is mainly controlled by the viscosity of the organic shell of the SOA, with the most sensitive viscosity region with respect to reactive uptake lying between 10^2 and 10^5 Pa s.¹⁴ When the viscosity of the organic shell is less than 10^2 Pa s, the reactive uptake of IEPOX through the organic coating is not impeded due to fast diffusion times. However, as the viscosity of the organic shell becomes larger than 10^5 Pa s, the reactive uptake is strongly limited by the IEPOX diffusion process within the

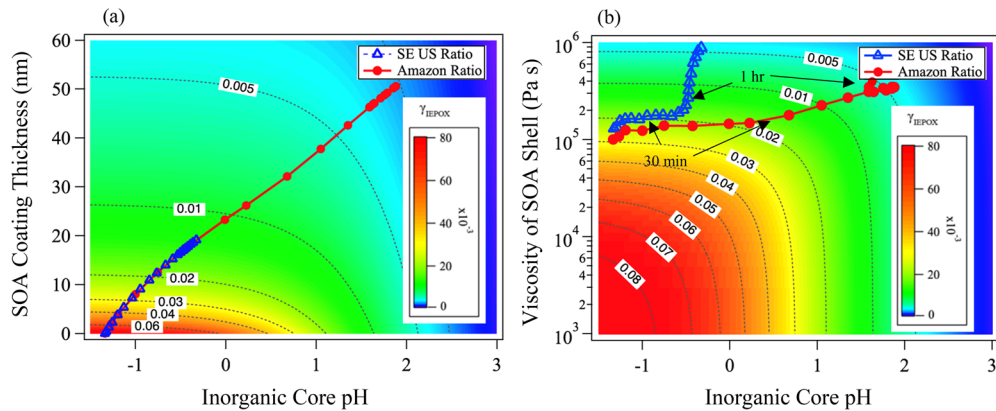


Figure 4. Effects of aerosol acidity (pH), IEPOX-derived SOA coating (shell) thickness, and SOA shell viscosity on the formation of IEPOX-derived SOA. Panel (a) shows that the IEPOX-derived SOA shell thickness and inorganic core acidity alters the reactive uptake coefficient of IEPOX (γ_{IEPOX}) onto the aerosols, assuming an average viscosity of $5 \times 10^5 \text{ Pa s}$. The blue triangles and red dots represent the measurements performed during experimental conditions mimicking the Southeastern United States and Amazon, respectively. The trend line (simple spline fit to guide the eye) suggests that, as the reaction proceeds, the SOA shell thickens with an increase of the core pH, thereby reducing the reactive uptake of IEPOX onto the aerosols and thus self-limiting any further SOA formation. Panel (b) shows the effects of SOA shell viscosity and inorganic core acidity on γ_{IEPOX} assuming an average SOA shell thickness of $\sim 15 \text{ nm}$ (on each side) based on field measurements in the Southeastern United States.¹⁴ The black arrows correspond to the elapsed time since the start of the IEPOX injection under each condition. The relatively large uncertainties in pH estimation shown in panel (b) toward the end of the experiment were due to extremely low inorganic sulfate concentrations from IEPOX reactive uptake. The color bar in panel (a) and (b) represents γ_{IEPOX} values from 1×10^{-4} to 8×10^{-2} .

IEPOX-derived SOA based on similar viscosities values in a previous study.¹⁴ Hence, the viscosity modeling results shown in Figure 3 suggest that as the IEPOX-derived SOA forms, it will impede the subsequent acid-catalyzed reactive uptake of IEPOX to existing aerosol, explaining (in part) the self-limitation of IEPOX yielding more SOA. The latter is especially true for aerosols formed under experimental conditions that mimic the Amazon, where daytime RH is between 50 and 60% during the dry season.¹⁵ Figure 3 also shows that the viscosity increases over the time scale of the experiments, and it is directly linked to the increased percentage of the total IEPOX-derived OSs in the particle phase, suggesting the importance of these low-volatility organic species in governing aerosol particle viscosity.⁹⁶ The viscosity values for particles that are homogeneously mixed are also estimated and presented in Figure S6. In cases where the particles are homogeneously mixed, the model results show that viscosity of the particle is much lower than that of the phase-separated organic shell due to the high hygroscopicity of the ABS particles. The extensive conversion of inorganic sulfate to OSs shown in Figures 3 and S3 also contributes to a higher viscosity value both in the core and in the shell, agreeing with similar measurements performed by Olson et al.¹⁶ as well as Raman measurements using markers that distinguish inorganic and organic sulfate from Bondy et al.⁸¹ The increase of the viscosity in the core was likely due to loss of water in the particles as the inorganic sulfate is converted to organic sulfate,^{68,82} while the increase of the viscosity in the shell could be attributed to the combined effects of less hygroscopic and more viscous organic components formed during the multi-phase chemical process.

3.4. Atmospheric Implications of IEPOX-Derived SOA Phase State on Partitioning and Chemical Reactivity.

The above model analyses show that the net effect of increasing viscosity for the organic coating of the IEPOX-derived SOA, together with the increasing pH of the aerosol core, reduces the reactive uptake of IEPOX. To quantify the contribution of each factor, a resistor model that contains these

three parameters as variables is used to describe the reactive uptake coefficient of IEPOX, γ_{IEPOX} , onto organic-coated inorganic aerosols:^{29,83}

$$\frac{1}{\gamma(a_{\text{H}^+}, l_{\text{org}}, D_{\text{org}})} = \frac{r_p \omega}{4D_{\text{gas}}} + \frac{1}{\alpha} + \frac{1}{\Gamma_{\text{aq}}(a_{\text{H}^+})} + \frac{1}{\Gamma_{\text{org}}(l_{\text{org}}, D_{\text{org}})} \quad (1)$$

In eq 1, $\frac{1}{\Gamma_{\text{aq}}}$ and $\frac{1}{\Gamma_{\text{org}}}$ are the terms controlling the reactive uptake process due to aerosol acidity and organic coating, respectively, which can each be calculated by

$$\frac{1}{\Gamma_{\text{aq}}(a_{\text{H}^+})} = \frac{S_a \omega}{4VRTH_{\text{aq}} k_{\text{aq}}(a_{\text{H}^+})} \quad (2)$$

$$\frac{1}{\Gamma_{\text{org}}(l_{\text{org}}, D_{\text{org}})} = \frac{\omega l_{\text{org}}}{4RTH_{\text{org}} D_{\text{org}}} \frac{r_c + l_{\text{org}}}{r_c} \quad (3)$$

In eq 1, r_c is the particle core radius, l_{org} is the thickness of the organic coating, ω is the mean velocity of IEPOX in the air (281 m s^{-1} at 298 K based on Riedel et al.),⁸⁴ S_a is the total surface area of the particles, and D_{gas} is the gas–particle diffusion coefficient and is $0.1 \text{ cm}^2 \text{ s}^{-1}$ based on a previous study.³⁶ The constant α is the mass accommodation coefficient of the sulfate core (0.1 based on Gaston et al.).³⁶

In eq 2, V is the total particle core volume calculated from the particle core size, R is the universal gas constant ($0.08205 \text{ L atm mol}^{-1} \text{ K}^{-1}$), H_{aq} is the Henry's law coefficient in the aqueous phase ($1 \times 10^6 \text{ M atm}^{-1}$ based on Budisulistiorini et al. and Gaston et al.),^{36,85} and k_{aq} is the first-order reaction rate constant in the aqueous phase, and can be calculated from Gaston et al. and Eddingsaas et al., as shown in the SI.^{36,86} In eq 3, l_{org} is the coating thickness (a variable depending on the reaction time during the experiment), H_{org} is the Henry's law coefficient in the organic layer ($6 \times 10^5 \text{ M atm}^{-1}$ based on

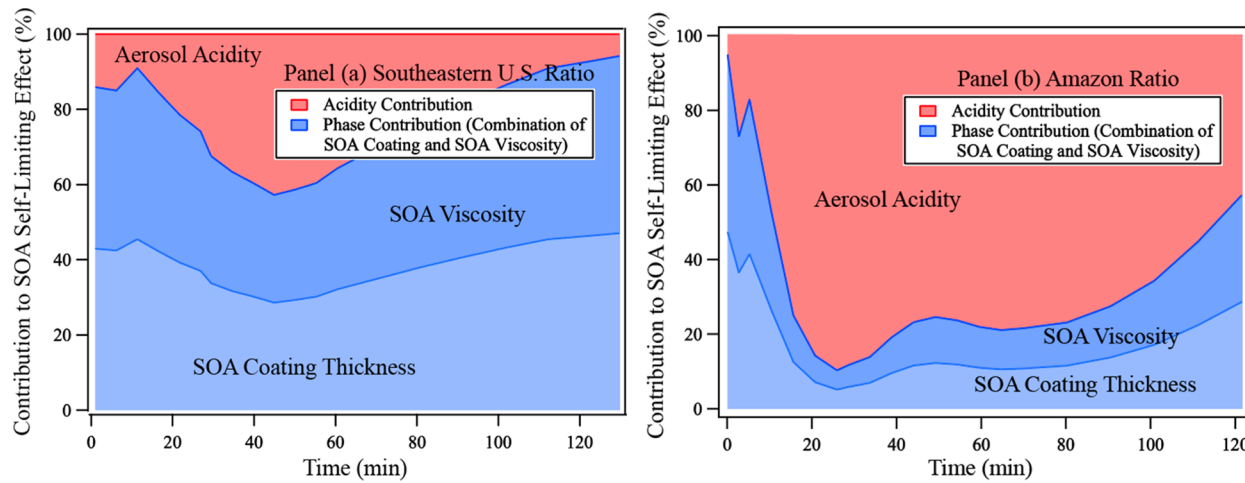


Figure 5. Relative contribution of each factor in changing the γ_{IEPOX} throughout the course of the IEPOX reactive uptake experiments, with the same time resolution as the experimental data in Figure 3. The red color shows the relative contribution from aerosol acidity, while the blue color shows the relative contribution from aerosol phase state, which is a combination of two factors (thickness and viscosity of the organic shell). The blue line separates the contribution of viscosity. Panel (a) shows the contributions of each factor during experimental conditions mimicking the Southeastern United States. Panel (b) shows the contributions of each factor during experimental conditions mimicking the Amazon.

Zhang et al.),¹⁴ D_{org} is the diffusion coefficient of IEPOX in the organic layer, and r_c is the radius of the acidic sulfate core.

Equation 1 shows that $\gamma_{\text{IEPOX}}(a_{\text{H}^+}, l_{\text{org}}, D_{\text{org}})$ is a nonlinear function of the aerosol core acidity, a_{H^+} , the IEPOX-derived SOA coating thickness, l_{org} and the diffusion coefficient of IEPOX within the organic shell, D_{org} , calculated from the viscosity value and the Stokes–Einstein equation.⁸⁷ Figure 4a shows the influence of organic shell (coating) thickness and core acidity on γ_{IEPOX} with respect to laboratory conditions mimicking Southeastern United States and the Amazon, assuming an average viscosity of $5 \times 10^5 \text{ Pa s}$ based on the viscosity values of the organic coating at 2 h reaction time. Modeled aerosols began with a pH value of -1.33 with no IEPOX-derived SOA coating, and SOA coating thickness and pH value of the core gradually increasing. The increase of both parameters leads to a decrease in γ_{IEPOX} suggesting a self-limited SOA growth rate. At lower pH values ($\text{pH} < 1.5$), the organic coating thickness dominates the change of the γ_{IEPOX} while the influence of acidity on γ_{IEPOX} becomes stronger at higher pH values ($\text{pH} > 1.5$). Figure 4b shows the interrelationship between organic shell viscosity and core acidity on γ_{IEPOX} when the IEPOX-derived SOA has a coating thickness of 15 nm, similar to the value estimated from field measurement¹⁴ (equivalent to ~ 50 and ~ 20 min of the Southeast United States and Amazon ratio experiments). The estimated aerosol viscosity and pH both contribute to the reduction of γ_{IEPOX} as the SOA forms.

The contribution of three factors, acidity, organic coating viscosity, and organic shell thickness, on γ_{IEPOX} during the course of the experiments is shown in Figure 5. Due to the nonlinear relationship between the above variables and γ_{IEPOX} , an univariate approach by comparing γ_{IEPOX} at each time stamp of the experiment with the γ_{IEPOX} at $t = 0$ with and without any of the three factors⁸⁸ is used to derive Figure 5. The contribution from each factor can be expressed in eqs 4–6:

$$p_{a_{\text{H}^+}} = \frac{\gamma_{\text{IEPOX}}(a_{\text{H}^+}, t_0, l_{\text{org}}, t, D_{\text{org}}, t) - \gamma_{\text{IEPOX}}(a_{\text{H}^+}, t, l_{\text{org}}, t, D_{\text{org}}, t)}{\gamma_{\text{IEPOX}}(a_{\text{H}^+}, l_{\text{org}}, D_{\text{org}}, t_0) - \gamma_{\text{IEPOX}}(a_{\text{H}^+}, l_{\text{org}}, D_{\text{org}}, t), t} \quad (4)$$

$$p_{l_{\text{org}}} = \frac{\gamma_{\text{IEPOX}}(a_{\text{H}^+}, t, l_{\text{org}}, t_0, D_{\text{org}}, t) - \gamma_{\text{IEPOX}}(a_{\text{H}^+}, t, l_{\text{org}}, t, D_{\text{org}}, t)}{\gamma_{\text{IEPOX}}(a_{\text{H}^+}, l_{\text{org}}, D_{\text{org}}, t_0) - \gamma_{\text{IEPOX}}(a_{\text{H}^+}, l_{\text{org}}, D_{\text{org}}, t), t} \quad (5)$$

$$p_{D_{\text{org}}} = \frac{\gamma_{\text{IEPOX}}(a_{\text{H}^+}, t, l_{\text{org}}, D_{\text{org}}, t_0) - \gamma_{\text{IEPOX}}(a_{\text{H}^+}, t, l_{\text{org}}, D_{\text{org}}, t)}{\gamma_{\text{IEPOX}}(a_{\text{H}^+}, l_{\text{org}}, D_{\text{org}}, t_0) - \gamma_{\text{IEPOX}}(a_{\text{H}^+}, l_{\text{org}}, D_{\text{org}}, t), t} \quad (6)$$

$$f_{a_{\text{H}^+}} = \frac{p_{a_{\text{H}^+}}}{p_{a_{\text{H}^+}} + p_{l_{\text{org}}} + p_{D_{\text{org}}}} \quad (7)$$

$$f_{l_{\text{org}}} = \frac{p_{l_{\text{org}}}}{p_{a_{\text{H}^+}} + p_{l_{\text{org}}} + p_{D_{\text{org}}}} \quad (8)$$

$$f_{D_{\text{org}}} = \frac{p_{D_{\text{org}}}}{p_{a_{\text{H}^+}} + p_{l_{\text{org}}} + p_{D_{\text{org}}}} \quad (9)$$

where $f_{a_{\text{H}^+}}$, $f_{l_{\text{org}}}$, and $f_{D_{\text{org}}}$ represent the normalized contributions of aerosol core acidity, organic shell thickness, and organic viscosity, respectively, to γ_{IEPOX} at any given time during the IEPOX reactive uptake process. And $p_{a_{\text{H}^+}}$, $p_{l_{\text{org}}}$, and $p_{D_{\text{org}}}$ represent the ratio of the contribution from aerosol core acidity, organic shell thickness, and organic viscosity, respectively, to γ_{IEPOX} at any given time during the IEPOX reactive uptake process. The terms $t = 0$ and $t = t_0$ represent the time right before IEPOX injection and the time stamp of interest, respectively, as shown in panels (c) and (d) in Figure 3. The reason why normalized contributions $f_{a_{\text{H}^+}}$, $f_{l_{\text{org}}}$, and $f_{D_{\text{org}}}$ are introduced is because the relationship between these variables and γ_{IEPOX} is nonlinear, making $p_{a_{\text{H}^+}} + p_{l_{\text{org}}} + p_{D_{\text{org}}}$ not necessarily equal to 100%. The results above demonstrate the contribution of each factor to the reduction of γ_{IEPOX} at each time stamp of the experiment. To obtain the contribution of the rate of changing acidity, organic shell thickness, and diffusion coefficient on the change of γ_{IEPOX} during the course of the experiments, the partial derivative of $\gamma_{\text{IEPOX}}(a_{\text{H}^+}, l_{\text{org}}, D_{\text{org}})$ with respect of each variable can be calculated to

represent the influences of the changing rate of each factor on γ_{IEPOX} , with results shown in [eqs S11–S13](#) and [Figure S7](#). The relationship between consumed inorganic sulfate and the pH of the inorganic sulfate core is described in [Figure S8](#) and [eq S14](#).

[Figure 5](#) shows the contribution of each factor to the change of γ_{IEPOX} for laboratory conditions mimicking both the Southeastern United States and Amazon. We attribute $f_{\text{a}_{\text{H}_2}}$ to acidity-induced contributions and the combination of $f_{\text{l}_{\text{org}}}$ and $f_{D_{\text{org}}}$ to phase state-induced contributions because the coating thickness and aerosol viscosity co-contribute to the phase state induced changes of aerosol production. During the experiments mimicking the Southeastern United States, the reduction of γ_{IEPOX} can be mainly attributed to the change of aerosol phase state, as the pH value of the inorganic core does not change much during the course of the experiments. In contrast, experimental conditions mimicking the Amazon reveal that aerosol acidity is responsible for more than 70% of the change of γ_{IEPOX} during most of the reaction times. The phase state of the organic shell has greater influence on γ_{IEPOX} for the first 10 min and after 1.5 h of the initial IEPOX injection, because the acidity did not change too much for the first 10 min and when the concentration of OSs (and their corresponding oligomers) is enhanced and pH is stable after 1.5 h, respectively. The results indicate that, at low IEPOX:SO₄²⁻ ratios, the self-limiting reactions of IEPOX-derived SOA are mainly caused by the change of aerosol phase state; however, as IEPOX concentration increases, the acidity of the aerosol core influences γ_{IEPOX} as the pH undergoes more drastic changes initially, followed by the phase state change due to the formation of OS monomers and oligomers thereof. Given that atmospheric aerosols have a residence time of about 1–2 weeks and often are mixed with both organic and inorganic components,^{89,90} the acidity and phase state may play important roles in the self-limiting process of IEPOX multiphase chemistry at different life stages of the aerosol particles. The results above assumed that the particles in the Southeastern United States and the Amazon forest have similar composition and initial pH values while the composition in the actual two locations may be different, and thus, affecting the initial pH of the inorganic particles.^{91,92} The uncertainty range of the Henry's law constant of IEPOX may also alter the contributions of the three factors above, warranting further study;^{14,36,85,93,94} however, the general trend should remain the same. It is worth noting that the viscous IEPOX-derived SOA and the reduced acidity of the aerosol core could also reduce the diffusion and reactive uptake of O₃, OH, and N₂O₅ species,^{29,35,95} thereby reducing other heterogeneous reactions and possibly prolonging the atmospheric lifetime of IEPOX-derived SOA. In addition, the rapid conversion from inorganic sulfate to organic sulfate also reduces the hygroscopicity of the aerosols, leading to a potential improvement in visibility under the same ambient humidity.

Our results indicate that the inorganic and organic components of aerosol particles jointly impact their physical and chemical properties, influencing the formation, evolution, and fate of ambient SOA. As described in this study, the formation of IEPOX-derived SOA significantly alters aerosol viscosity and acidity, affecting subsequent multiphase chemistry and composition of particles. The phase state and acidity changes due to the formation of IEPOX-derived SOA are the dominant parameters for the self-limiting effect of IEPOX

reactive uptake, depending on the initial IEPOX:SO₄²⁻ ratio. All in all, the strong effect of IEPOX on aerosol physical and chemical properties could also have substantial impacts on how other SOA types form in isoprene-rich regions.

■ ASSOCIATED CONTENT

S Supporting Information

The Supporting Information is available free of charge at <https://pubs.acs.org/doi/10.1021/acsearthspacechem.9b00209>.

UNC smog chamber operation conditions, the modeling details of the aerosol pH, the viscosity calculation procedures, and how the effects of the acidity and viscosity on IEPOX-derived SOA formation was calculated; glass transition temperatures used for viscosity modeling; four scenarios of modeling used in this study; parameters used for acidity modeling; Q values at each time step of the experiment; schematic diagram of the IEPOX-derived SOA generation on acidic inorganic sulfate particles in the environmental chamber; morphology of the particles after the IEPOX uptake; acidity estimation of the particles under the four scenarios; acidity estimation based on different pK_a values of the OSs; viscosities of the aerosols based on the four scenarios discussed above; contribution of changing acidity, viscosity, and coating thickness on the reactive uptake of IEPOX; model parameterization of acidity and the fraction of IEPOX-derived organosulfates (PDF)

■ AUTHOR INFORMATION

Corresponding Authors

*Email: surratt@unc.edu. Phone: (919) 966-0470. Fax: (919) 966-7911.

*Email: aulta@umich.edu. Phone: (734) 763-2283. Fax: (734) 647-4865.

*Email: yzhang01@live.unc.edu. Phone: (919) 966-3861. Fax: (919) 966-7911.

ORCID

Yuzhi Chen: [0000-0002-2547-8428](https://orcid.org/0000-0002-2547-8428)

Nicole E. Olson: [0000-0003-1600-8050](https://orcid.org/0000-0003-1600-8050)

Matthieu Riva: [0000-0003-0054-4131](https://orcid.org/0000-0003-0054-4131)

Timothy B. Onasch: [0000-0001-7796-7840](https://orcid.org/0000-0001-7796-7840)

Jesse H. Kroll: [0000-0002-6275-521X](https://orcid.org/0000-0002-6275-521X)

Andrew P. Ault: [0000-0002-7313-8559](https://orcid.org/0000-0002-7313-8559)

Jason D. Surratt: [0000-0002-6833-1450](https://orcid.org/0000-0002-6833-1450)

Notes

The authors declare no competing financial interest.

■ ACKNOWLEDGMENTS

This work was funded by the National Science Foundation (NSF) under Atmospheric and Geospace Sciences (AGS) Grants 1703535 (J.D.S.), 1703019 (A.P.A.), and 1638672 (J.H.K.). This work is also funded in part by the NSF Postdoctoral Fellowship under AGS Grant 1524731 (Y.Z.) and the National Institutes of Health (NIH) grant no. T32ES007018. A.R.K. acknowledges support from the Dreyfus Postdoctoral Program in Environmental Chemistry. The authors acknowledge the Michigan Center for Materials Characterization (MC²) for use of the SEM instruments and staff assistance, as well as the Scanning Probe Microscopy

Facility in the Department of Chemistry at the University of Michigan. We acknowledge Charles E. Kolb for useful discussions and assistance when drafting the manuscript. We also acknowledge Hahaha O. T. Pye, Manishkumar B. Shrivastava, Hongyu Guo, Lu Shen, Eric Dong, and Zhe Peng for useful discussions.

■ REFERENCES

- (1) Seinfeld, J. H.; Pandis, S. N. *Atmospheric Chemistry and Physics*; John Wiley & Sons: Hoboken, NJ, 2016.
- (2) Jimenez, J. L.; Canagaratna, M. R.; Donahue, N. M.; Prevot, A. S. H.; Zhang, Q.; Kroll, J. H.; DeCarlo, P. F.; Allan, J. D.; Coe, H.; Ng, N. L.; Aiken, A. C.; Docherty, K. S.; Ulbrich, I. M.; Grieshop, A. P.; Robinson, A. L.; Duplissy, J.; Smith, J. D.; Wilson, K. R.; Lanz, V. A.; Hueglin, C.; Sun, Y. L.; Tian, J.; Laaksonen, A.; Raatikainen, T.; Rautiainen, J.; Vaattovaara, P.; Ehn, M.; Kulmala, M.; Tomlinson, J. M.; Collins, D. R.; Cubison, M. J.; Dunlea, J. E.; Huffman, J. A.; Onasch, T. B.; Alfarra, M. R.; Williams, P. I.; Bower, K.; Kondo, Y.; Schneider, J.; Drewnick, F.; Borrmann, S.; Weimer, S.; Demerjian, K.; Salcedo, D.; Cottrell, L.; Griffin, R.; Takami, A.; Miyoshi, T.; Hatakeyama, S.; Shimono, A.; Sun, J. Y.; Zhang, Y. M.; Dzepina, K.; Kimmel, J. R.; Sueper, D.; Jayne, J. T.; Herndon, S. C.; Trimborn, A. M.; Williams, L. R.; Wood, E. C.; Middlebrook, A. M.; Kolb, C. E.; Baltensperger, U.; Worsnop, D. R. Evolution of organic aerosols in the atmosphere. *Science* **2009**, *326* (5959), 1525–1529.
- (3) Kroll, J. H.; Seinfeld, J. H. Chemistry of secondary organic aerosol: Formation and evolution of low-volatility organics in the atmosphere. *Atmos. Environ.* **2008**, *42* (16), 3593–3624.
- (4) Zhang, Y.; Gong, Z.; Sa, S. d.; Bateman, A. P.; Liu, Y.; Li, Y.; Geiger, F. M.; Martin, S. T. Production and Measurement of Organic Particulate Matter in the Harvard Environmental Chamber. *J. Visualized Exp.* **2018**, *141*, No. e55685.
- (5) Ng, N. L.; Canagaratna, M. R.; Zhang, Q.; Jimenez, J. L.; Tian, J.; Ulbrich, I. M.; Kroll, J. H.; Docherty, K. S.; Chhabra, P. S.; Bahreini, R.; Murphy, S. M.; Seinfeld, J. H.; Hildebrandt, L.; Donahue, N. M.; DeCarlo, P. F.; Lanz, V. A.; Prévôt, A. S. H.; Dinar, E.; Rudich, Y.; Worsnop, D. R. Organic aerosol components observed in Northern Hemispheric datasets from Aerosol Mass Spectrometry. *Atmos. Chem. Phys.* **2010**, *10* (10), 4625–4641.
- (6) Surratt, J. D.; Murphy, S. M.; Kroll, J. H.; Ng, N. L.; Hildebrandt, L.; Sorooshian, A.; Szmigielski, R.; Vermeylen, R.; Maenhaut, W.; Claeys, M.; Flagan, R. C.; Seinfeld, J. H. Chemical composition of secondary organic aerosol formed from the photooxidation of isoprene. *J. Phys. Chem. A* **2006**, *110* (31), 9665–9690.
- (7) Kroll, J. H.; Ng, N. L.; Murphy, S. M.; Flagan, R. C.; Seinfeld, J. H. Secondary organic aerosol formation from isoprene photooxidation. *Environ. Sci. Technol.* **2006**, *40* (6), 1869–1877.
- (8) Guenther, A. B.; Jiang, X.; Heald, C. L.; Sakulyanontvittaya, T.; Duhl, T.; Emmons, L. K.; Wang, X. The Model of Emissions of Gases and Aerosols from Nature version 2.1 (MEGAN2.1): an extended and updated framework for modeling biogenic emissions. *Geosci. Model Dev.* **2012**, *5* (6), 1471–1492.
- (9) Surratt, J. D.; Chan, A. W.; Eddingsaas, N. C.; Chan, M.; Loza, C. L.; Kwan, A. J.; Hersey, S. P.; Flagan, R. C.; Wennberg, P. O.; Seinfeld, J. H. Reactive intermediates revealed in secondary organic aerosol formation from isoprene. *Proc. Natl. Acad. Sci. U. S. A.* **2010**, *107* (15), 6640–6645.
- (10) Budisulistiorini, S. H.; Baumann, K.; Edgerton, E. S.; Bairai, S. T.; Mueller, S.; Shaw, S. L.; Knipping, E. M.; Gold, A.; Surratt, J. D. Seasonal characterization of submicron aerosol chemical composition and organic aerosol sources in the southeastern United States: Atlanta, Georgia, and Look Rock, Tennessee. *Atmos. Chem. Phys.* **2016**, *16* (8), 5171–5189.
- (11) Xu, L.; Guo, H.; Boyd, C. M.; Klein, M.; Bougiatioti, A.; Cerully, K. M.; Hite, J. R.; Isaacman-VanWertz, G.; Kreisberg, N. M.; Knot, C.; Olson, K.; Koss, A.; Goldstein, A. H.; Hering, S. V.; de Gouw, J.; Baumann, K.; Lee, S.-H.; Nenes, A.; Weber, R. J.; Ng, N. L. Effects of anthropogenic emissions on aerosol formation from isoprene and monoterpenes in the southeastern United States. *Proc. Natl. Acad. Sci. U. S. A.* **2015**, *112* (1), 37–42.
- (12) de Sá, S. S.; Palm, B. B.; Campuzano-Jost, P.; Day, D. A.; Newburn, M. K.; Hu, W.; Isaacman-VanWertz, G.; Yee, L. D.; Thalman, R.; Brito, J.; Carbone, S.; Artaxo, P.; Goldstein, A. H.; Manzi, A. O.; Souza, R. A. F.; Mei, F.; Shilling, J. E.; Springston, S. R.; Wang, J.; Surratt, J. D.; Alexander, M. L.; Jimenez, J. L.; Martin, S. T. Influence of urban pollution on the production of organic particulate matter from isoprene epoxydiols in central Amazonia. *Atmos. Chem. Phys.* **2017**, *17* (11), 6611–6629.
- (13) Lin, Y. H.; Zhang, H.; Pye, H. O.; Zhang, Z.; Marth, W. J.; Park, S.; Arashiro, M.; Cui, T.; Budisulistiorini, S. H.; Sexton, K. G.; Vizuete, W.; Xie, Y.; Luecken, D. J.; Piletic, I. R.; Edney, E. O.; Bartolotti, L. J.; Gold, A.; Surratt, J. D. Epoxide as a precursor to secondary organic aerosol formation from isoprene photooxidation in the presence of nitrogen oxides. *Proc. Natl. Acad. Sci. U. S. A.* **2013**, *110* (17), 6718–6723.
- (14) Zhang, Y.; Chen, Y.; Lambe, A. T.; Olson, N. E.; Lei, Z.; Craig, R. L.; Zhang, Z.; Gold, A.; Onasch, T. B.; Jayne, J. T.; Worsnop, D. R.; Gaston, C. J.; Thornton, J. A.; Vizuete, W.; Ault, A. P.; Surratt, J. D. Effect of Aerosol-Phase State on Secondary Organic Aerosol Formation from the Reactive Uptake of Isoprene-Derived Epoxydiols (IEPOX). *Environ. Sci. Technol. Lett.* **2018**, *5* (3), 167–174.
- (15) Riva, M.; Chen, Y.; Zhang, Y.; Lei, Z.; Olson, N.; Boyer, H. C.; Narayan, S.; Yee, L. D.; Green, H.; Cui, T.; Zhang, Z.; Baumann, K. D.; Fort, M.; Edgerton, E. S.; Budisulistiorini, S.; Rose, C. A.; Ribeiro, I.; Oliveira, R. L.; Santos, E.; Szopa, S.; Machado, C.; Zhao, Y.; Alves, E.; de Sa, S.; Hu, W.; Knipping, E.; Shaw, S.; Duvoisin Junior, S.; Souza, R. A. F. d.; Palm, B. B.; Jimenez, J. L.; Glasius, M.; Goldstein, A. H.; Pye, H. O. T.; Gold, A.; Turpin, B. J.; Vizuete, W.; Martin, S. T.; Thornton, J.; Dutcher, C. S.; Ault, A. P.; Surratt, J. D. Increasing Isoprene Epoxydiol-to-Inorganic Sulfate Aerosol (IEPOX-Sulfinate) Ratio Results in Extensive Conversion of Inorganic Sulfate to Organosulfur Forms: Implications for Aerosol Physicochemical Properties. *Environ. Sci. Technol.* **2019**, *53* (15), 8682–8694.
- (16) Olson, N. E.; Lei, Z.; Craig, R. L.; Zhang, Y.; Chen, Y.; Lambe, A. T.; Zhang, Z.; Gold, A.; Surratt, J. D.; Ault, A. P. Reactive Uptake of Isoprene Epoxydiols Increases the Viscosity of the Core of Phase-Separated Aerosol Particles. *ACS Earth and Space Chemistry* **2019**, *3* (8), 1402–1414.
- (17) Virtanen, A.; Joutsensaari, J.; Koop, T.; Kannisto, J.; Yli-Pirila, P.; Leskinen, J.; Makela, J. M.; Holopainen, J. K.; Poschl, U.; Kulmala, M.; Worsnop, D. R.; Laaksonen, A. An amorphous solid state of biogenic secondary organic aerosol particles. *Nature* **2010**, *467* (7317), 824–827.
- (18) Renbaum-Wolff, L.; Grayson, J. W.; Bateman, A. P.; Kuwata, M.; Sellier, M.; Murray, B. J.; Shilling, J. E.; Martin, S. T.; Bertram, A. K. Viscosity of α -pinene secondary organic material and implications for particle growth and reactivity. *Proc. Natl. Acad. Sci. U. S. A.* **2013**, *110* (20), 8014–8019.
- (19) Koop, T.; Bookhold, J.; Shiraiwa, M.; Poschl, U. Glass transition and phase state of organic compounds: dependency on molecular properties and implications for secondary organic aerosols in the atmosphere. *Phys. Chem. Chem. Phys.* **2011**, *13* (43), 19238–19255.
- (20) Virtanen, A.; Kannisto, J.; Kuuluvainen, H.; Arffman, A.; Joutsensaari, J.; Saukko, E.; Hao, L.; Yli-Pirila, P.; Tiitta, P.; Holopainen, J. K.; Keskinen, J.; Worsnop, D. R.; Smith, J. N.; Laaksonen, A. Bounce behavior of freshly nucleated biogenic secondary organic aerosol particles. *Atmos. Chem. Phys.* **2011**, *11* (16), 8759–8766.
- (21) Shiraiwa, M.; Yee, L. D.; Schilling, K. A.; Loza, C. L.; Craven, J. S.; Zuend, A.; Ziemann, P. J.; Seinfeld, J. H. Size distribution dynamics reveal particle-phase chemistry in organic aerosol formation. *Proc. Natl. Acad. Sci. U. S. A.* **2013**, *110* (29), 11746–11750.
- (22) Shiraiwa, M.; Berkemeier, T.; Schilling-Fahnestock, K. A.; Seinfeld, J. H.; Poschl, U. Molecular corridors and kinetic regimes in the multiphase chemical evolution of secondary organic aerosols. *Atmos. Chem. Phys.* **2014**, *14* (16), 8323–8341.

- (23) Slade, J. H.; Ault, A. P.; Bui, A. T.; Ditto, J. C.; Lei, Z.; Bondy, A. L.; Olson, N. E.; Cook, R. D.; Desrochers, S. J.; Harvey, R. M.; Erickson, M. H.; Wallace, H. W.; Alvarez, S. L.; Flynn, J. H.; Boor, B. E.; Petrucci, G. A.; Gentner, D. R.; Griffin, R. J.; Shepson, P. B. Bouncier Particles at Night: Biogenic Secondary Organic Aerosol Chemistry and Sulfate Drive Diel Variations in the Aerosol Phase in a Mixed Forest. *Environ. Sci. Technol.* **2019**, *53* (9), 4977–4987.
- (24) Reid, J. P.; Bertram, A. K.; Topping, D. O.; Laskin, A.; Martin, S. T.; Petters, M. D.; Pope, F. D.; Rovelli, G. The viscosity of atmospherically relevant organic particles. *Nat. Commun.* **2018**, *9* (1), 956.
- (25) Smith, M. L.; Bertram, A. K.; Martin, S. T. Deliquescence, efflorescence, and phase miscibility of mixed particles of ammonium sulfate and isoprene-derived secondary organic material. *Atmos. Chem. Phys.* **2012**, *12* (20), 9613–9628.
- (26) You, Y.; Renbaum-Wolff, L.; Carreras-Sospedra, M.; Hanna, S. J.; Hiranuma, N.; Kamal, S.; Smith, M. L.; Zhang, X.; Weber, R. J.; Shilling, J. E.; Dabab, D.; Martin, S. T.; Bertram, A. K. Images reveal that atmospheric particles can undergo liquid–liquid phase separations. *Proc. Natl. Acad. Sci. U. S. A.* **2012**, *109* (33), 13188–13193.
- (27) Shrestha, M.; Zhang, Y.; Upshur, M. A.; Liu, P.; Blair, S. L.; Wang, H.; Nizkorodov, S. A.; Thomson, R. J.; Martin, S. T.; Geiger, F. M. On surface order and disorder of α -pinene-derived secondary organic material. *J. Phys. Chem. A* **2015**, *119* (19), 4609–4617.
- (28) Zhou, S.; Hwang, B. C. H.; Lakey, P. S. J.; Zuend, A.; Abbatt, J. P. D.; Shiraiwa, M. Multiphase reactivity of polycyclic aromatic hydrocarbons is driven by phase separation and diffusion limitations. *Proc. Natl. Acad. Sci. U. S. A.* **2019**, *116* (24), 11658–11663.
- (29) Gaston, C. J.; Thornton, J. A.; Ng, N. L. Reactive uptake of N_2O_5 to internally mixed inorganic and organic particles: the role of organic carbon oxidation state and inferred organic phase separations. *Atmos. Chem. Phys.* **2014**, *14* (11), 5693–5707.
- (30) Zhang, Y.; Liu, P.; Gong, Z.; Geiger, F. M.; Martin, S. T. Production and Measurement of Organic Particulate Matter in a Flow Tube Reactor. *J. Visualized Exp.* **2018**, *142*, No. e55684.
- (31) Drozd, G. T.; Woo, J. L.; McNeill, V. F. Self-limited uptake of α -pinene oxide to acidic aerosol: the effects of liquid–liquid phase separation and implications for the formation of secondary organic aerosol and organosulfates from epoxides. *Atmos. Chem. Phys.* **2013**, *13* (16), 8255–8263.
- (32) Stewart, D. J.; Cai, C.; Nayler, J.; Preston, T. C.; Reid, J. P.; Krieger, U. K.; Marcolli, C.; Zhang, Y. H. Liquid–Liquid Phase Separation in Mixed Organic/Inorganic Single Aqueous Aerosol Droplets. *J. Phys. Chem. A* **2015**, *119* (18), 4177–4190.
- (33) Riva, M.; Bell, D. M.; Hansen, A.-M. K.; Drozd, G. T.; Zhang, Z.; Gold, A.; Imre, D.; Surratt, J. D.; Glasius, M.; Zelenyuk, A. Effect of Organic Coatings, Humidity and Aerosol Acidity on Multiphase Chemistry of Isoprene Epoxydiols. *Environ. Sci. Technol.* **2016**, *50* (11), 5580–5588.
- (34) Taketani, F.; Kanaya, Y.; Akimoto, H. Kinetics of HO_2 Uptake in Levoglucosan and Polystyrene Latex Particles. *J. Phys. Chem. Lett.* **2010**, *1* (11), 1701–1704.
- (35) Slade, J. H.; Knopf, D. A. Multiphase OH oxidation kinetics of organic aerosol: the role of particle phase state and relative humidity. *Geophys. Res. Lett.* **2014**, *41* (14), 5297–5306.
- (36) Gaston, C. J.; Riedel, T. P.; Zhang, Z.; Gold, A.; Surratt, J. D.; Thornton, J. A. Reactive Uptake of an Isoprene-Derived Epoxydiol to Submicron Aerosol Particles. *Environ. Sci. Technol.* **2014**, *48* (19), 11178–11186.
- (37) Pöschl, U.; Shiraiwa, M. Multiphase Chemistry at the Atmosphere–Biosphere Interface Influencing Climate and Public Health in the Anthropocene. *Chem. Rev.* **2015**, *115* (10), 4440–4475.
- (38) Donaldson, M. A.; Bish, D. L.; Raff, J. D. Soil surface acidity plays a determining role in the atmospheric-terrestrial exchange of nitrous acid. *Proc. Natl. Acad. Sci. U. S. A.* **2014**, *111* (52), 18472–18477.
- (39) Guo, H.; Otjes, R.; Schlag, P.; Kiendler-Scharr, A.; Nenes, A.; Weber, R. J. Effectiveness of ammonia reduction on control of fine particle nitrate. *Atmos. Chem. Phys.* **2018**, *18* (16), 12241–12256.
- (40) Rindelaub, J. D.; McAvey, K. M.; Shepson, P. B. The photochemical production of organic nitrates from α -pinene and loss via acid-dependent particle phase hydrolysis. *Atmos. Environ.* **2015**, *100*, 193–201.
- (41) Surratt, J. D.; Lewandowski, M.; Offenberg, J. H.; Jaoui, M.; Kleindienst, T. E.; Edney, E. O.; Seinfeld, J. H. Effect of Acidity on Secondary Organic Aerosol Formation from Isoprene. *Environ. Sci. Technol.* **2007**, *41* (15), 5363–5369.
- (42) Surratt, J. D.; Gómez-González, Y.; Chan, A. W. H.; Vermeylen, R.; Shahgholi, M.; Kleindienst, T. E.; Edney, E. O.; Offenberg, J. H.; Lewandowski, M.; Jaoui, M.; Maenhaut, W.; Claeys, M.; Flagan, R. C.; Seinfeld, J. H. Organosulfate Formation in Biogenic Secondary Organic Aerosol. *J. Phys. Chem. A* **2008**, *112* (36), 8345–8378.
- (43) Craig, R. L.; Peterson, P. K.; Nandy, L.; Lei, Z.; Hossain, M. A.; Camarena, S.; Dodson, R. A.; Cook, R. D.; Dutcher, C. S.; Ault, A. P. Direct Determination of Aerosol pH: Size-Resolved Measurements of Submicrometer and Supermicrometer Aqueous Particles. *Anal. Chem.* **2018**, *90* (19), 11232–11239.
- (44) Rindelaub, J. D.; Craig, R. L.; Nandy, L.; Bondy, A. L.; Dutcher, C. S.; Shepson, P. B.; Ault, A. P. Direct Measurement of pH in Individual Particles via Raman Microspectroscopy and Variation in Acidity with Relative Humidity. *J. Phys. Chem. A* **2016**, *120* (6), 911–917.
- (45) Craig, R. L.; Nandy, L.; Axson, J. L.; Dutcher, C. S.; Ault, A. P. Spectroscopic Determination of Aerosol pH from Acid–Base Equilibria in Inorganic, Organic, and Mixed Systems. *J. Phys. Chem. A* **2017**, *121* (30), 5690–5699.
- (46) Hennigan, C. J.; Izumi, J.; Sullivan, A. P.; Weber, R. J.; Nenes, A. A critical evaluation of proxy methods used to estimate the acidity of atmospheric particles. *Atmos. Chem. Phys.* **2015**, *15* (5), 2775–2790.
- (47) Guo, H.; Xu, L.; Bougiatioti, A.; Cerully, K. M.; Capps, S. L.; Hite, J. R., Jr.; Carlton, A. G.; Lee, S. H.; Bergin, M. H.; Ng, N. L.; Nenes, A.; Weber, R. J. Fine-particle water and pH in the southeastern United States. *Atmos. Chem. Phys.* **2015**, *15* (9), 5211–5228.
- (48) Ault, A. P.; Moffet, R. C.; Baltrušaitis, J.; Collins, D. B.; Ruppel, M. J.; Cuadra-Rodriguez, L. A.; Zhao, D.; Guasco, T. L.; Ebben, C. J.; Geiger, F. M.; Bertram, T. H.; Prather, K. A.; Grassian, V. H. Size-Dependent Changes in Sea Spray Aerosol Composition and Properties with Different Seawater Conditions. *Environ. Sci. Technol.* **2013**, *47* (11), 5603–5612.
- (49) Pye, H. O. T.; Zuend, A.; Fry, J. L.; Isaacman-VanWertz, G.; Capps, S. L.; Appel, K. W.; Foroutan, H.; Xu, L.; Ng, N. L.; Goldstein, A. H. Coupling of organic and inorganic aerosol systems and the effect on gas–particle partitioning in the southeastern US. *Atmos. Chem. Phys.* **2018**, *18* (1), 357–370.
- (50) Dallemande, M. A.; Huang, X. Y.; Eddingsaas, N. C. Variation in pH of Model Secondary Organic Aerosol during Liquid–Liquid Phase Separation. *J. Phys. Chem. A* **2016**, *120* (18), 2868–2876.
- (51) Riedel, T. P.; Lin, Y. H.; Zhang, Z.; Chu, K.; Thornton, J. A.; Vizuete, W.; Gold, A.; Surratt, J. D. Constraining condensed-phase formation kinetics of secondary organic aerosol components from isoprene epoxydiols. *Atmos. Chem. Phys.* **2016**, *16* (3), 1245–1254.
- (52) Isaacman-VanWertz, G.; Massoli, P.; O’Brien, R.; Lim, C.; Franklin, J. P.; Moss, J. A.; Hunter, J. F.; Nowak, J. B.; Canagaratna, M. R.; Misztal, P. K.; Arata, C.; Roscioli, J. R.; Herndon, S. T.; Onasch, T. B.; Lambe, A. T.; Jayne, J. T.; Su, L.; Knopf, D. A.; Goldstein, A. H.; Worsnop, D. R.; Kroll, J. H. Chemical evolution of atmospheric organic carbon over multiple generations of oxidation. *Nat. Chem.* **2018**, *10* (4), 462–468.
- (53) Hunter, J. F.; Carrasquillo, A. J.; Daumit, K. E.; Kroll, J. H. Secondary Organic Aerosol Formation from Acyclic, Monocyclic, and Polycyclic Alkanes. *Environ. Sci. Technol.* **2014**, *48* (17), 10227–10234.
- (54) Zhang, Z.; Lin, Y. H.; Zhang, H.; Surratt, J. D.; Ball, L. M.; Gold, A. Technical Note: Synthesis of isoprene atmospheric oxidation

- products: isomeric epoxydiols and the rearrangement products *cis*- and *trans*-3-methyl-3,4-dihydroxytetrahydrofuran. *Atmos. Chem. Phys.* **2012**, *12* (18), 8529–8535.
- (55) Lin, Y. H.; Zhang, Z.; Docherty, K. S.; Zhang, H.; Budisulistiorini, S. H.; Rubitschun, C. L.; Shaw, S. L.; Knipping, E. M.; Edgerton, E. S.; Kleindienst, T. E.; Gold, A.; Surratt, J. D. Isoprene epoxydiols as precursors to secondary organic aerosol formation: acid-catalyzed reactive uptake studies with authentic compounds. *Environ. Sci. Technol.* **2012**, *46* (1), 250–258.
- (56) Cui, T.; Zeng, Z.; dos Santos, E. O.; Zhang, Z.; Chen, Y.; Zhang, Y.; Rose, C. A.; Budisulistiorini, S. H.; Collins, L. B.; Bodnar, W. M.; de Souza, R. A. F.; Martin, S. T.; Machado, C. M. D.; Turpin, B. J.; Gold, A.; Ault, A. P.; Surratt, J. D. Development of a hydrophilic interaction liquid chromatography (HILIC) method for the chemical characterization of water-soluble isoprene epoxydiol (IEPOX)-derived secondary organic aerosol. *Environmental Science: Processes & Impacts* **2018**, *20* (11), 1524–1536.
- (57) Laskina, O.; Morris, H. S.; Grandquist, J. R.; Estillore, A. D.; Stone, E. A.; Grassian, V. H.; Tivanski, A. V. Substrate-Deposited Sea Spray Aerosol Particles: Influence of Analytical Method, Substrate, and Storage Conditions on Particle Size, Phase, and Morphology. *Environ. Sci. Technol.* **2015**, *49* (22), 13447–13453.
- (58) Bondy, A. L.; Bonanno, D.; Moffet, R. C.; Wang, B.; Laskin, A.; Ault, A. P. Diverse Chemical Mixing States of Aerosol Particles in the Southeastern United States. *Atmos. Chem. Phys.* **2018**, *18* (16), 12595–12612.
- (59) DeRieux, W. S. W.; Li, Y.; Lin, P.; Laskin, J.; Laskin, A.; Bertram, A. K.; Nizkorodov, S. A.; Shiraiwa, M. Predicting the glass transition temperature and viscosity of secondary organic material using molecular composition. *Atmos. Chem. Phys.* **2018**, *18* (9), 6331–6351.
- (60) Zhang, Y.; Katira, S.; Lee, A.; Lambe, A. T.; Onasch, T. B.; Xu, W.; Brooks, W. A.; Canagaratna, M. R.; Freedman, A.; Jayne, J. T.; Worsnop, D. R.; Davidovits, P.; Chandler, D.; Kolb, C. E. Kinetically controlled glass transition measurement of organic aerosol thin films using broadband dielectric spectroscopy. *Atmos. Meas. Tech.* **2018**, *11* (6), 3479–3490.
- (61) Li, Y.; Shiraiwa, M. Timescales of secondary organic aerosols to reach equilibrium at various temperatures and relative humidities. *Atmos. Chem. Phys.* **2019**, *19* (9), 5959–5971.
- (62) Lessmeier, J.; Dette, H. P.; Godt, A.; Koop, T. Physical state of 2-methylbutane-1,2,3,4-tetraol in pure and internally mixed aerosols. *Atmos. Chem. Phys.* **2018**, *18* (21), 15841–15857.
- (63) Dette, H. P.; Qi, M.; Schröder, D. C.; Godt, A.; Koop, T. Glass-Forming Properties of 3-Methylbutane-1,2,3-tricarboxylic Acid and Its Mixtures with Water and Pinonic Acid. *J. Phys. Chem. A* **2014**, *118* (34), 7024–7033.
- (64) Dette, H. P.; Koop, T. Glass Formation Processes in Mixed Inorganic/Organic Aerosol Particles. *J. Phys. Chem. A* **2015**, *119* (19), 4552–4561.
- (65) Wexler, A. S.; Clegg, S. L. Atmospheric aerosol models for systems including the ions H^+ , NH_4^+ , Na^+ , SO_4^{2-} , NO_3^- , Cl^- , Br^- , and H_2O . *J. Geophys. Res.* **2002**, *107* (D14), 4207.
- (66) Nazaroff, W. W.; Alvarez-Cohen, L. *Environmental Engineering Science*; Wiley: New York, 2001.
- (67) Varutbangkul, V.; Brechtel, F. J.; Bahreini, R.; Ng, N. L.; Keywood, M. D.; Kroll, J. H.; Flagan, R. C.; Seinfeld, J. H.; Lee, A.; Goldstein, A. H. Hygroscopicity of secondary organic aerosols formed by oxidation of cycloalkenes, monoterpenes, sesquiterpenes, and related compounds. *Atmos. Chem. Phys.* **2006**, *6* (9), 2367–2388.
- (68) Estillore, A. D.; Hettiyadura, A. P. S.; Qin, Z.; Leckrone, E.; Wombacher, B.; Humphry, T.; Stone, E. A.; Grassian, V. H. Water Uptake and Hygroscopic Growth of Organosulfate Aerosol. *Environ. Sci. Technol.* **2016**, *50* (8), 4259–4268.
- (69) Zuend, A.; Marcolli, C.; Luo, B. P.; Peter, T. A thermodynamic model of mixed organic-inorganic aerosols to predict activity coefficients. *Atmos. Chem. Phys.* **2008**, *8* (16), 4559–4593.
- (70) Clegg, S. L.; Brimblecombe, P.; Wexler, A. S. Thermodynamic Model of the System $\text{H}^+ - \text{NH}_4^+ - \text{SO}_4^{2-} - \text{NO}_3^- - \text{H}_2\text{O}$ at Tropospheric Temperatures. *J. Phys. Chem. A* **1998**, *102* (12), 2137–2154.
- (71) Zuend, A.; Seinfeld, J. H. Modeling the gas-particle partitioning of secondary organic aerosol: the importance of liquid-liquid phase separation. *Atmos. Chem. Phys.* **2012**, *12* (9), 3857–3882.
- (72) Zuend, A.; Marcolli, C.; Booth, A. M.; Lienhard, D. M.; Soonsin, V.; Krieger, U. K.; Topping, D. O.; McFiggans, G.; Peter, T.; Seinfeld, J. H. New and extended parameterization of the thermodynamic model AIOMFAC: calculation of activity coefficients for organic-inorganic mixtures containing carboxyl, hydroxyl, carbonyl, ether, ester, alkenyl, alkyl, and aromatic functional groups. *Atmos. Chem. Phys.* **2011**, *11* (17), 9155–9206.
- (73) Saleh, R.; Khlystov, A. Determination of Activity Coefficients of Semi-Volatile Organic Aerosols Using the Integrated Volume Method. *Aerosol Sci. Technol.* **2009**, *43* (8), 838–846.
- (74) Bondy, A. L.; Kirpes, R. M.; Merzel, R. L.; Pratt, K. A.; Banaszak Holl, M. M.; Ault, A. P. Atomic Force Microscopy-Infrared Spectroscopy of Individual Atmospheric Aerosol Particles: Subdiffraction Limit Vibrational Spectroscopy and Morphological Analysis. *Anal. Chem.* **2017**, *89* (17), 8594–8598.
- (75) Sobanska, S.; Falgayrac, G.; Rimetz-Planchon, J.; Perdrix, E.; Bremard, C.; Barbillat, J. Resolving the internal structure of individual atmospheric aerosol particle by the combination of Atomic Force Microscopy, ESEM-EDX, Raman and ToF-SIMS imaging. *Microchem. J.* **2014**, *114*, 89–98.
- (76) Hettiyadura, A. P. S.; Stone, E. A.; Kundu, S.; Baker, Z.; Geddes, E.; Richards, K.; Humphry, T. Determination of atmospheric organosulfates using HILIC chromatography with MS detection. *Atmos. Meas. Tech.* **2015**, *8* (6), 2347–2358.
- (77) Hettiyadura, A. P. S.; Al-Naiema, I. M.; Hughes, D. D.; Fang, T.; Stone, E. A. Organosulfates in Atlanta, Georgia: anthropogenic influences on biogenic secondary organic aerosol formation. *Atmos. Chem. Phys.* **2019**, *19* (5), 3191–3206.
- (78) Fountoukis, C.; Nenes, A. ISORROPIA II: a computationally efficient thermodynamic equilibrium model for $\text{K}^+ - \text{Ca}^{2+} - \text{Mg}^{2+} - \text{NH}_4^+ - \text{Na}^+ - \text{SO}_4^{2-} - \text{NO}_3^- - \text{Cl}^- - \text{H}_2\text{O}$ aerosols. *Atmos. Chem. Phys.* **2007**, *7* (17), 4639–4659.
- (79) Lopez-Hilfiker, F. D.; Mohr, C.; D'Ambro, E. L.; Lutz, A.; Riedel, T. P.; Gaston, C. J.; Iyer, S.; Zhang, Z.; Gold, A.; Surratt, J. D.; Lee, B. H.; Kurten, T.; Hu, W. W.; Jimenez, J.; Hallquist, M.; Thornton, J. A. Molecular Composition and Volatility of Organic Aerosol in the Southeastern U.S.: Implications for IEPOX Derived SOA. *Environ. Sci. Technol.* **2016**, *50* (5), 2200–2209.
- (80) Hu, W.; Palm, B. B.; Day, D. A.; Campuzano-Jost, P.; Krechmer, J. E.; Peng, Z.; de Sá, S. S.; Martin, S. T.; Alexander, M. L.; Baumann, K.; Hacker, L.; Kiendler-Scharr, A.; Koss, A. R.; de Gouw, J. A.; Goldstein, A. H.; Seco, R.; Sjostedt, S. J.; Park, J. H.; Guenther, A. B.; Kim, S.; Canonaco, F.; Prévôt, A. S. H.; Brune, W. H.; Jimenez, J. L. Volatility and lifetime against OH heterogeneous reaction of ambient isoprene-epoxydiols-derived secondary organic aerosols (IEPOX-SOA). *Atmos. Chem. Phys.* **2016**, *16* (18), 11563–11580.
- (81) Bondy, A. L.; Craig, R. L.; Zhang, Z.; Gold, A.; Surratt, J. D.; Ault, A. P. Isoprene-Derived Organosulfates: Vibrational Mode Analysis by Raman Spectroscopy, Acidity-Dependent Spectral Modes, and Observation in Individual Atmospheric Particles. *J. Phys. Chem. A* **2018**, *122* (1), 303–315.
- (82) Hansen, A. M. K.; Hong, J.; Raatikainen, T.; Kristensen, K.; Ylisirniö, A.; Virtanen, A.; Petäjä, T.; Glasius, M.; Prisle, N. L. Hygroscopic properties and cloud condensation nuclei activation of limonene-derived organosulfates and their mixtures with ammonium sulfate. *Atmos. Chem. Phys.* **2015**, *15* (24), 14071–14089.
- (83) Anttila, T.; Kiendler-Scharr, A.; Tillmann, R.; Mentel, T. F. On the Reactive Uptake of Gaseous Compounds by Organic-Coated Aqueous Aerosols: Theoretical Analysis and Application to the Heterogeneous Hydrolysis of N_2O_5 . *J. Phys. Chem. A* **2006**, *110* (35), 10435–10443.
- (84) Riedel, T. P.; Lin, Y.-H.; Budisulistiorini, S. H.; Gaston, C. J.; Thornton, J. A.; Zhang, Z.; Vizuete, W.; Gold, A.; Surratt, J. D.

Heterogeneous Reactions of Isoprene-Derived Epoxides: Reaction Probabilities and Molar Secondary Organic Aerosol Yield Estimates. *Environ. Sci. Technol. Lett.* **2015**, 2 (2), 38–42.

(85) Budisulistiorini, S. H.; Nenes, A.; Carlton, A. G.; Surratt, J. D.; McNeill, V. F.; Pye, H. O. T. Simulating Aqueous-Phase Isoprene-Epoxydiol (IEPOX) Secondary Organic Aerosol Production During the 2013 Southern Oxidant and Aerosol Study (SOAS). *Environ. Sci. Technol.* **2017**, 51 (9), 5026–5034.

(86) Eddingsaas, N. C.; VanderVelde, D. G.; Wennberg, P. O. Kinetics and Products of the Acid-Catalyzed Ring-Opening of Atmospherically Relevant Butyl Epoxy Alcohols. *J. Phys. Chem. A* **2010**, 114 (31), 8106–8113.

(87) Shiraiwa, M.; Ammann, M.; Koop, T.; Pöschl, U. Gas uptake and chemical aging of semisolid organic aerosol particles. *Proc. Natl. Acad. Sci. U. S. A.* **2011**, 108 (27), 11003–11008.

(88) Rencher, A. C.; Scott, D. T. Assessing the contribution of individual variables following rejection of a multivariate hypothesis. *Communications in Statistics - Simulation and Computation* **1990**, 19 (2), 535–553.

(89) Dlugosz-Lisiecka, M.; Bem, H. Determination of the mean aerosol residence times in the atmosphere and additional (210)Po input on the base of simultaneous determination of (7)Be, (22)Na, (210)Pb, (210)Bi and (210)Po in urban air. *J. Radioanal. Nucl. Chem.* **2012**, 293 (1), 135–140.

(90) Ault, A. P.; Axson, J. L. Atmospheric Aerosol Chemistry: Spectroscopic and Microscopic Advances. *Anal. Chem.* **2017**, 89 (1), 430–452.

(91) Shrivastava, M.; Andreae, M. O.; Artaxo, P.; Barbosa, H. M. J.; Berg, L. K.; Brito, J.; Ching, J.; Easter, R. C.; Fan, J.; Fast, J. D.; Feng, Z.; Fuentes, J. D.; Glasius, M.; Goldstein, A. H.; Alves, E. G.; Gomes, H.; Gu, D.; Guenther, A.; Jathar, S. H.; Kim, S.; Liu, Y.; Lou, S.; Martin, S. T.; McNeill, V. F.; Medeiros, A.; de Sá, S. S.; Shilling, J. E.; Springston, S. R.; Souza, R. A. F.; Thornton, J. A.; Isaacman-VanWertz, G.; Yee, L. D.; Ynoue, R.; Zaveri, R. A.; Zelenyuk, A.; Zhao, C. Urban pollution greatly enhances formation of natural aerosols over the Amazon rainforest. *Nat. Commun.* **2019**, 10 (1), 1046.

(92) Weber, R. J.; Guo, H.; Russell, A. G.; Nenes, A. High aerosol acidity despite declining atmospheric sulfate concentrations over the past 15 years. *Nat. Geosci.* **2016**, 9 (4), 282–285.

(93) Woo, J. L.; McNeill, V. F. simpleGAMMA v1.0 – a reduced model of secondary organic aerosol formation in the aqueous aerosol phase (aaSOA). *Geosci. Model Dev.* **2015**, 8 (6), 1821–1829.

(94) McNeill, V. F. Aqueous Organic Chemistry in the Atmosphere: Sources and Chemical Processing of Organic Aerosols. *Environ. Sci. Technol.* **2015**, 49 (3), 1237–1244.

(95) Shrestha, M.; Zhang, Y.; Ebbin, C. J.; Martin, S. T.; Geiger, F. M. Vibrational sum frequency generation spectroscopy of secondary organic material produced by condensational growth from α -pinene ozonolysis. *J. Phys. Chem. A* **2013**, 117 (35), 8427–8436.

(96) Zhang, Y.; Nichman, L.; Spencer, P.; Jung, J. I.; Lee, A.; Heffernan, B. K.; Gold, A.; Zhang, Z.; Chen, Y.; Canagaratna, M. R.; Jayne, J. T.; Worsnop, D. R.; Onasch, T. B.; Surratt, J. D.; Chandler, D.; Davidovits, P.; Kolb, C. E. The Cooling Rate- and Volatility-Dependent Glass-Forming Properties of Organic Aerosols Measured by Broadband Dielectric Spectroscopy. *Environ. Sci. Technol.* **2019**, 53, 12366.